

CNWRA *A center of excellence in earth sciences and engineering*

A Division of Southwest Research Institute™
6220 Culebra Road • San Antonio, Texas, U.S.A. 78228-5166
(210) 522-5160 • Fax (210) 522-5155

July 3, 2001
Contract No. NRC-02-97-009

U.S. Nuclear Regulatory Commission
ATTN: Mrs. Deborah DeMarco
Office of Nuclear Material Safety and Safeguards
Two White Flint North
Mail Stop 8A23
Washington, DC 20555

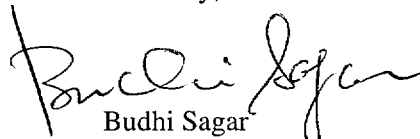
Subject: Dilational normal faults manuscript

Dear Mrs. DeMarco:

The attached manuscript is an outgrowth of work done through the Southwest Research Institute's Internal Research and Development Program. This work identifies a new way that normal faults control the flow of groundwater and hydrocarbons. When the fault plane transitions from a weak rock to a stronger rock the fault plane may be refracted, or bent slightly. This bend produces a zone of dilation in the stronger rock that may result in a migration pathway in saturated rocks or an infiltration pathway in the unsaturated zone. The results of this study, although conducted in Carbonate rocks in Texas, may be applicable to groundwater studies at Yucca Mountain. This copy of the manuscript is sent to you for informational purposes only and does not require NRC acceptance.

If you have any questions please contact Dr. David Ferrill at (210) 522-6082 or me at (210) 522-5252.

Sincerely,

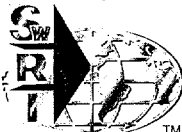

Budhi Sagar
Technical Director

rae

Attachment

J. Linehan	E. Whitt	S. Wastler	W. Patrick
W. Reamer	B. Meehan	T. Essig	CNWRA Dirs/EMs
B. Leslie	J. Greeves	D. Brooks	T. Nagy (SwRI Contracts)
D. DeMarco	J. Piccone	P. Justus	D. Ferrill
			A. Morris

D:\GLGP Group\letters\misc\NRD-07-03-2001\hlm.wpd



Washington Office • Twinbrook Metro Plaza #210
12300 Twinbrook Parkway • Rockville, Maryland 20852-1606

Dilational normal faults

David A. Ferrill¹, Alan P. Morris²

¹ CNWRA, Southwest Research Institute, 6220 Culebra Road, San Antonio, TX 78238

² Department of Earth and Environmental Science, University of Texas at San Antonio, San Antonio, TX 78249

Abstract – At low differential effective stress and with minimum principal compressive effective stress near or below zero, rocks fail in multiple modes and with variable failure angles. Under these conditions mechanical stratigraphy exerts a significant influence on initial, small-displacement, normal fault dip. Less competent layers fail in shear mode along fractures that approximate the failure angle predicted by a standard rock-mechanics analysis. Deformation of more competent layers, which is driven in part by interaction with the more rapidly deforming incompetent layers, produces hybrid mode failure in which failure angles are smaller than in shear mode. Analyses of small normal faults cutting Cretaceous carbonate strata in west Texas indicate that fault geometries resulting from this effect commonly display dilational jogs where the fault traverses more competent beds. Similar dilational jogs along faults within carbonates of the Cretaceous-age Edwards Group near San Antonio, Texas have been enlarged by groundwater flow, and are important permeability and shallow infiltration structures.

1. Introduction

Normal faults in stratified rocks commonly have dip changes that are visible in dip-parallel profiles. Variation in normal fault dip can be caused by various mechanisms, including; (i) differential compaction of sedimentary layers after fault formation (Xiao and Suppe, 1989); (ii) active fault deformation (e.g., by slip or shear along layering or intersecting faults; Ferrill et al., 1998; Ferrill et al., 2000); (iii) linkage of an originally vertically-segmented fault (Childs et al., 1996; Mansfield and Cartwright, 1996); and (iv) fault initiation with failure angles controlled by rock mechanical properties and effective stresses at the time of failure (Mandl, 1988; Peacock and Sanderson, 1992).

We describe outcrop-scale normal faults in Cretaceous carbonate strata in west Texas where characteristic fault dips are associated with particular lithologic units. These faults lack diagnostic traits of passive deformation (differential compaction) or active deformation (e.g., slip or shear along layering), or of development from originally vertically segmented faults. We interpret the dip changes to be primary features of the faults, developed during fault nucleation and growth, and controlled by the failure mode and failure angle of the mechanical layers experiencing the faulting. Finally, we use examples of faults with dip changes in Edwards aquifer strata in central Texas to illustrate the importance of dilation on steep fault segments to groundwater infiltration and flow.

2. Background

The angle of shear failure (θ , measured between the maximum principal compressive stress and the failure plane) in rock can be predicted from the angle of internal friction (friction angle, φ) using the following equation (Mandl, 1988):

$$\theta = \pm (45 - \varphi/2) \quad \text{Eqn. 1}$$

Failure mode depends upon the effective differential stress and the effective minimum principal compressive stress at the time of failure, and upon the strength characteristics of the rock (Fig. 1). There are three general possibilities:

- (1) Shear failure, in which displacement is parallel to the fracture surface, and the normal stress acting on the fracture surface, $\sigma_3 < \sigma_n \geq 0$. The failure angle for this mode is given by equation 1 (Fig. 1a).
- (2) Tensile failure (“mode I”, e.g., Twiss and Moores, 1992), in which displacement is perpendicular to the fracture surface. In this case $\sigma_3 = \sigma_n < 0$ and $|\sigma_3| \geq$ tensile strength of the rock. The failure angle for this mode is 0° (Fig. 1b).
- (3) Hybrid failure, in which displacement is oblique to the fracture surface (“dilatant faults,” Mandl, 1988). In this case $\sigma_3 < \sigma_n < 0$ and $|\sigma_3| < \text{tensile strength of the rock}$. The failure angle for this mode lies between 0° and the angle predicted by equation 1 (Fig. 1c).

3. Analysis of natural examples from west Texas, U.S.A.

Horizontal to gently dipping layers of the Cretaceous Buda Limestone, exposed along Interstate Highway 10 (I-10), in west Texas are cut by small-displacement normal faults. At a roadcut exposure along eastbound I-10 at mile marker 195 (approximately 16 km west of Balmorhea, Texas), several faults have consistent dip changes through the various limestone layers (Fig. 2a). Layers in the outcrop dip gently, between horizontal and 10° , and dip changes of a few degrees are accommodated by the occurrence of faults described here.

3.1. *Fault shapes*

Faults are undulatory, cutting layering at $80\text{--}90^\circ$ in the more competent layers (K and H; Figs. 2 b through e and Table 1), and generally $65\text{--}75^\circ$ in less competent layers. Fault dip changes tend to be gradual rather than abrupt (Figs. 2 a through e). Slip on the faults produced normal offset, was approximately parallel to more shallowly dipping fault segments, and produced dilation at steep fault segments within the more competent layers. In the context of normal slip parallel to the more gently dipping fault segments, the steep segments are dilational jogs, equivalent to releasing bends. In one case, a small dissolution cavity has formed, suggesting localized groundwater flow along the dilational jog (also see Sibson, 1996).

3.2. *Fault zones*

Fault zone materials consist of a combination of crystalline calcite veins, rock fragments, and clay sized material (Fig. 3a). Along the releasing bend walls, veins of milky calcite (up to 5 cm thick) are locally present (Fig. 3b). Calcite crystals in these veins range from 5–15mm

across, and in some cases have euhedral terminations toward the vein centers. Along slip surfaces, coarse calcite veins that are well bonded with the wall rock are common. These veins are typically 2–5 mm thick, and consist of equant to elongate crystals 2–5 mm across. The core of the fault zones generally consists of angular to rounded carbonate rock fragments (1–30 mm diameter) and clayey (some iron rich) material (Fig. 3b). The filling tends to be amorphous, especially in fault releasing bends, but in some cases the fill is layered parallel to the walls along fault segments that parallel the slip direction. Tan colored, fine grained calcite veneer is common on wall rock interfaces and on open fracture surfaces within the fault zone. This finely crystalline material has the appearance of flowstone and suggests precipitation along open cavity walls under unsaturated conditions.

3.3 *Interpretation*

Failure angles for competent rocks undergoing shear tend to be on the order of 10–20° for competent rocks, and 15–45° for less competent rocks (Mandl, 1988). These angles decrease to 0° for hybrid failure modes (Fig. 1). If we assume that faulting initiated when layering was horizontal, then the angles between the faults and bedding represent the initial fault dips and the failure angle for each fault segment is 90°-fault segment dip (Table 1). The faults investigated here failed at a range of angles from 0–40°, and individual mechanical layers consistently failed at similar angles where cut by the four faults analyzed (Table 1). The lowest failure angles are indicative of competent rock failing in the hybrid mode, and is manifest by the dilational sense of displacement (see layers K and H in Figs. 2b through e and 3a and b; Mandl, 1988). Net slip on the faults from west Texas presented here was parallel to the sections with shallower dips.

Consequently, the subvertical fault sections dilated an amount equal to the fault-perpendicular component of fault slip.

3.4. *Origin of fault dip variation*

Variations of fault dip are the result of variations in the mechanical strength of rock layers coupled with low values of differential effective stress and a minimum principal compressive stress (σ_3) that is weakly compressive to tensile (Fig. 4). These conditions cause different layers to fail in different modes, hence generating different fracture orientations from bed to bed.

Initially, the stress state within a weaker layer generates shear failure (stress state A, Fig. 4). When the propagating tip of the shear fracture reaches the stronger layer, traction between the deforming weaker layer and the as yet undeformed stronger layer causes stress magnification in stronger layer. Because the stronger layer will not fail at the same differential stress level as the weaker layer, the differential stress increases as σ_3 decreases (becomes increasingly tensile or negative). The vertical σ_1 is unchanged because it is a function of the overlying rock. Ultimately, deformation of the weaker layer generates a large enough differential stress for the stronger layer to fail in hybrid mode (stress state B, Fig. 4). A consequence of failure occurring under different conditions in the two layers is that the failure angle in each layer is different, specifically, the failure angle in the stronger layer is smaller than that in the weaker layer (Fig. 4). This can be thought of as refraction of the fault trajectory as the fracture propagates through the rock mass. In general, the optimal fracture trajectory will be shorter in stronger layers than in weaker layers.

The stress conditions illustrated in Fig. 4 are those for unsaturated carbonate rocks at depths of about 250–300 meters. A similar situation could arise in saturated conditions where the pore fluid pressure is sufficiently elevated to generate a tensile σ_3 , and differential effective stress is low enough to straddle the shear failure/hybrid failure transition.

3.5. *Slip tendency analysis*

Slip tendency is the ratio of resolved shear stress to resolved normal stress on a surface (Morris et al., 1996). At the time of sliding, slip tendency equals the frictional resistance to sliding on the surface. Slip tendency analysis of these fault yields the results illustrated in Fig. 5. The σ_3 direction is approximately ENE–WSW (070°) which corresponds to the extension experienced by west Texas as the southern Basin and Range and Rio Grande Rift developed during the late Tertiary. In this analysis, we assume a simple Andersonian normal faulting regime, with the magnitude of the intermediate principal compressive stress centered between the maximum and minimum compressive stress magnitudes. The steeper faults shown in profile as blue lines have low resolved normal stress and low resolved shear stress - therefore they are in low slip tendency orientations. These steep fault segments, approximately perpendicular to σ_3 have a very high dilation tendency (Ferrill et al., 1999). High dilation tendency segments tend to dilate in response to the same stress field that produces slip on the less steep fault segments.

4. Discussion

Net slip parallel to fault segments with lower dips causes steep fault segments to be releasing bends or dilational jogs. These dilational jogs locally enhance fault permeability.

Small-displacement normal faults in Edwards aquifer strata from the Balcones Fault system near San Antonio Texas exhibit dip changes at lithologic boundaries, similar to the examples from west Texas (Fig. 6). These faults also slipped parallel to lower dip segments, producing dilation of steep segments.

For vertical dilational fault segments, fracture porosity increase equals horizontal extension magnitude (Fig. 7). Dilational jogs on small-displacement normal faults within the Edwards aquifer are common sites of dissolution features (Figs. 6a and b). Because faults can propagate through mechanically heterogeneous sequences, they tend to produce both vertically and laterally connected flow pathways. Where these faults intersect the ground surface, they may be important pathways for shallow infiltration of groundwater (Fig. 7). In the case of the Edwards aquifer, the enhancement of flow pathways by dissolution is increased by the fact that the weaker, lower-fault-dip layers are clay rich compared with the stronger, steeper-fault-dip layers. Both the bed and the fault segment in the clay-rich layers have low permeability which leads to ponding of water within the dilational jog, thus increasing its exposure to dissolution.

5. Conclusions

Rock failure in a mechanically layered sequence at shallow depths or high fluid pressures results in variable failure angle. These variations in failure angle are caused by differences in friction angle or failure mode from layer to layer. Faults that cut several mechanical layers will have dip changes or will appear to “refract.” The resulting refracted fault trajectories can therefore yield information about mechanical stratigraphy. Conversely, knowledge of mechanical stratigraphy and stress conditions at the time of failure can be used to make predictions of fault

trajectories through a rock sequence. Refracted fault trajectories favor the development of dilational normal faults, which can develop in mechanically heterogeneous rock sequences by slip on faults cutting layers with different failure angles or different failure modes. Dilational normal faulting significantly enhances vertical infiltration at the surface and along strike pathways for flow in the subsurface.

Acknowledgments

This work was funded by Southwest Research Institute through the SwRI Internal Research and Development Program (project #20.R9223.01.001), and supported by the Center for Water Research at the University of Texas at San Antonio. We thank Larry McKague and English Percy for helpful reviews, and Rebecca Emmot and Cheryl Patton for preparation of the manuscript.

References

- Childs, C., Nicol, A., Walsh, J.J., Watterson, J., 1996. Growth of vertically segmented normal faults. *Journal of Structural Geology* 18, 1389–1397.
- Ferrill, D.A., Morris, A.P., Jones, S.M., Stamatakos, J.A., 1998. Extensional layer parallel shear and normal faulting. *Journal of Structural Geology* 20, 355–362.
- Ferrill, D.A., Winterle, J., Wittmeyer, G., Sims, D.W., Colton, S. Armstrong, A., Morris. A.P., 1999. Stressed rock strains groundwater at Yucca Mountain, Nevada. *GSA Today* 9(5): 1–8.

- Ferrill, D.A., Morris, A.P., Sims, D.W., Stamatakos, J.A. 2000. Crossing conjugate normal faults. *American Association of Petroleum Geologists Bulletin* 84 (10), 1543–1559.
- Goodman, R.E., 1980. *Introduction to Rock Mechanics*. John Wiley and Sons. 478 pp.
- Hoek, E., Brown, E.T., 1988. The Hoek-Brown Failure Criterion—A 1988 Update. 15th Canadian Rock Mechanics Symposium, pp. 31–38.
- Mandl, G., 1988. *Mechanics of Tectonic Faulting*. Elsevier, New York.
- Mansfield, C.S., Cartwright, J.A., 1996. High resolution fault displacement mapping from three-dimensional seismic data: evidence for dip linkage during fault growth. *Journal of Structural Geology* 18, 249–263.
- Morris, A.P., Ferrill, D.A., Henderson, D.B., 1996. Slip tendency analysis and fault reactivation. *Geology* 24, 275–278.
- Peacock, D.C.P., Sanderson, D.J., 1992. Effects of layering and anisotropy on fault geometry. *Journal of the Geological Society, London* 149, 793–802.
- Sibson, R.H. 1996. Structural permeability of fluid-driven fault-fracture meshes. *Journal of Structural Geology* 18, 1031–1042.
- Twiss, R.J., Moores, E.M. 1992. *Structural Geology*. W.H. Freeman and Company, New York. 532 pp.
- Xiao, H., Suppe, J. 1989. Role of compaction in the listric shape of growth normal faults. *American Association of Petroleum Geologists Bulletin* 73 (6), 777–786.

Figure Captions

Fig. 1. Mohr-space diagrams with Hoek-Brown failure envelope illustrating different failure modes: (a) shear failure, (b) tensile failure, (c) hybrid failure.

Fig. 2. Field photographs showing normal faults cutting limestone layers in the Buda Limestone, along I-10 east near Balmorhea, Texas. Field Notebook, 12 cm × 19 cm for scale. (a) Horst between northeast-dipping fault (4) and southwest-dipping fault (5). (b) Northeast-dipping horst-bounding fault (4) with 9 cm displacement. (c) Southwest-dipping horst-bounding fault (5) has 77 cm displacement. Note major and minor releasing bends and that horizontal dilation across releasing bends equals heave component of fault slip. (d) Northeast-dipping fault (8) has 7 cm displacement near base of exposure, and loses displacement upward to a tip in layer J. (e) Southwest-dipping fault (10) has 15 cm displacement near base of exposure, and loses displacement upward to a tip in layer J.

Fig. 3. Details of fault zone and releasing-bend-filling material along southwest dipping fault 5, (see Fig. 2c). Note coarse calcite vein fill along walls of releasing bend visible in (b).

Fig. 4. Mohr-space diagram illustrating how contrasting mechanical stratigraphy leads to different failure mode and failure angles in different layers. A stronger rock (e.g., Tavernalle Limestone) is more likely to fail in hybrid mode than a weaker rock (e.g., Bedford Limestone)

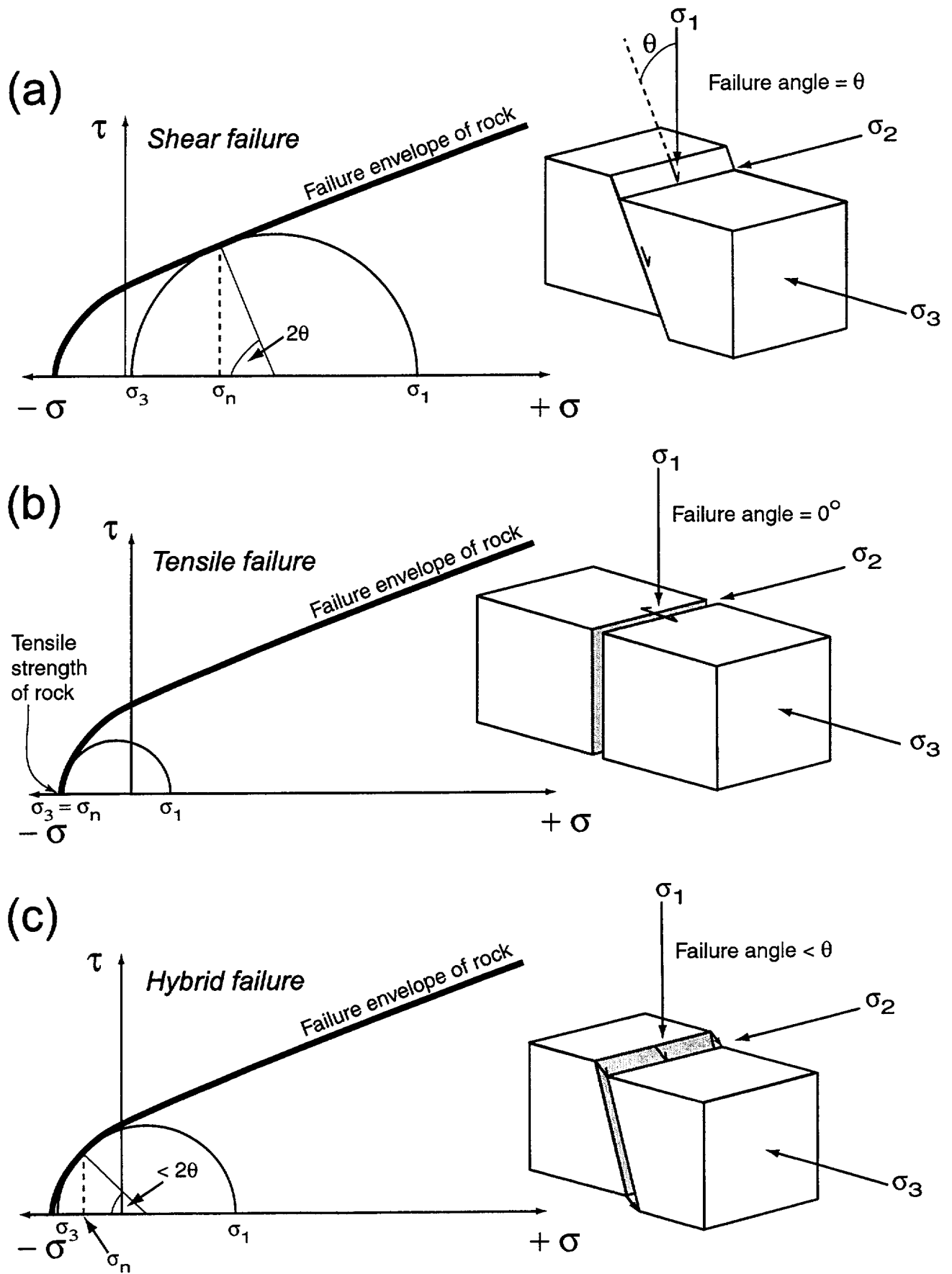
under the same normal faulting stress regime. See text for details. Equation and rock-quality parameters for generating failure envelopes from Hoek and Brown, 1988; rock strength data from Goodman, 1980, Table 3.1)

Fig. 5. Slip tendency analysis for faults illustrated in Figs. 2 and 3. Slip tendency plot for faults measured in the Balmorhea exposure. $\sigma_2 = 65\%$ of σ_1 ; $\sigma_3 = 30\%$ of σ_1 ; σ_1 is vertical; σ_2 horizontal, azimuth 160; σ_3 horizontal, azimuth 070. (a) Slip tendency plot illustrates the pattern of slip tendency, and triangles represent poles (dip corrected) to fault planes illustrated in Fig. 2 and tabulated in Table 1. (b) Cross sectional profile of fault geometry color coded according to slip tendency in interpreted stress field at time of faulting as shown in (a).

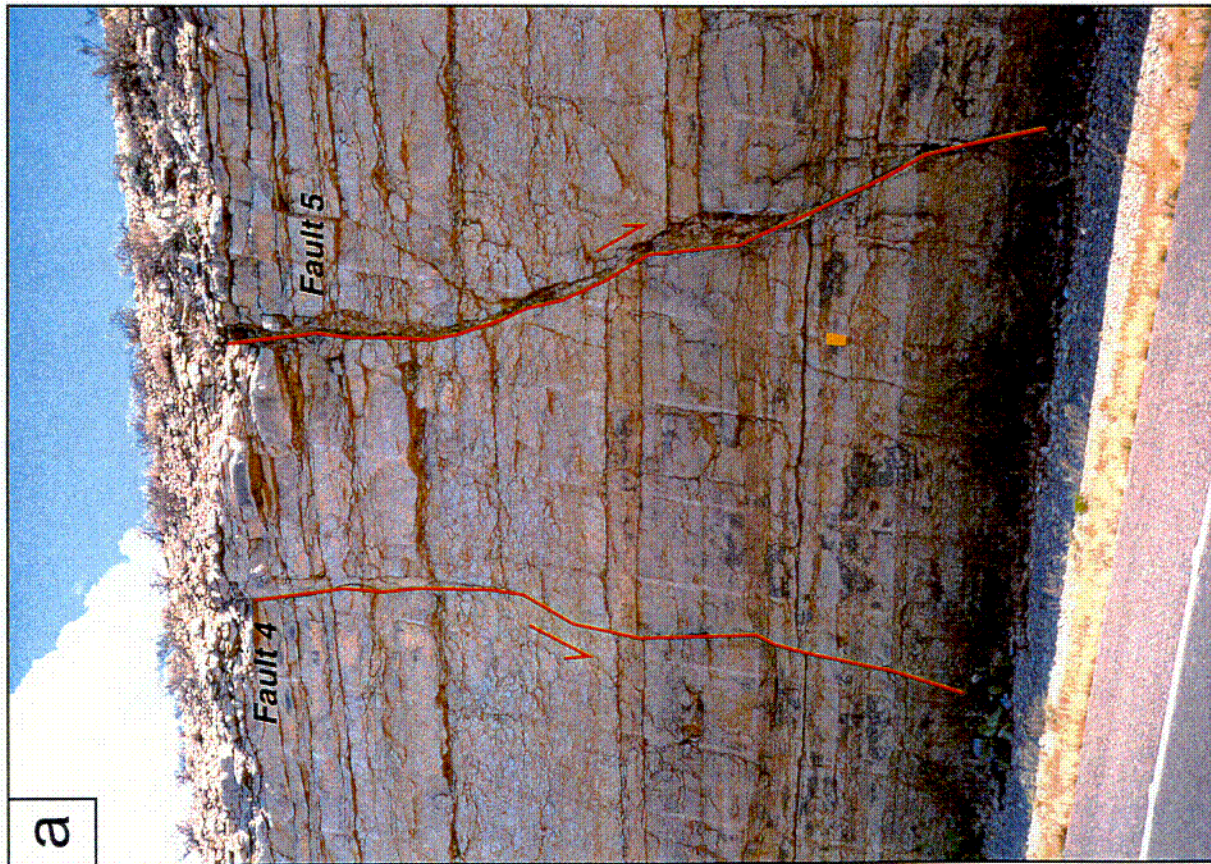
Fig. 6(a) and (b). Small-displacement normal faults in the Kainer Formation of the Edwards Group Limestone exposed in the Balcones Fault Zone, along State Route 211, approximately 1 km south of San Geronimo, Texas. Note that dissolution cavities are localized at steep, dilational segments of faults. Lens cap (5.5 cm diameter) for scale.

Fig. 7. Block diagram illustrating the role of dilational fault segments in shallow infiltration and subsurface groundwater flow.

Table 1. Fault segment and bedding orientation data for faults in the Balmorhea exposure. Failure angle is calculated assuming that faulting initiated when strata were horizontal. Unit subdivisions are based on lithologic properties and mechanical behavior.



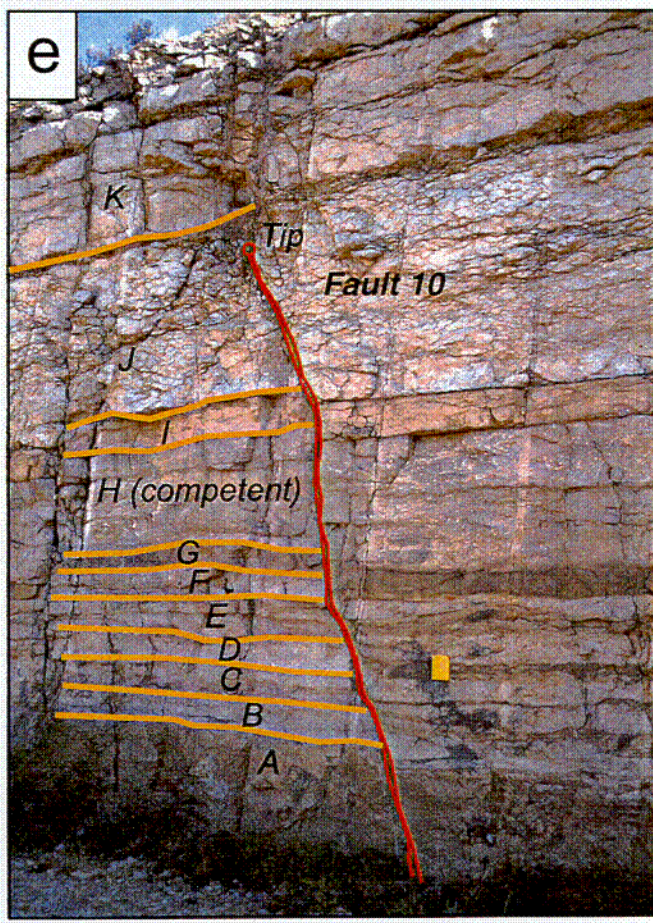
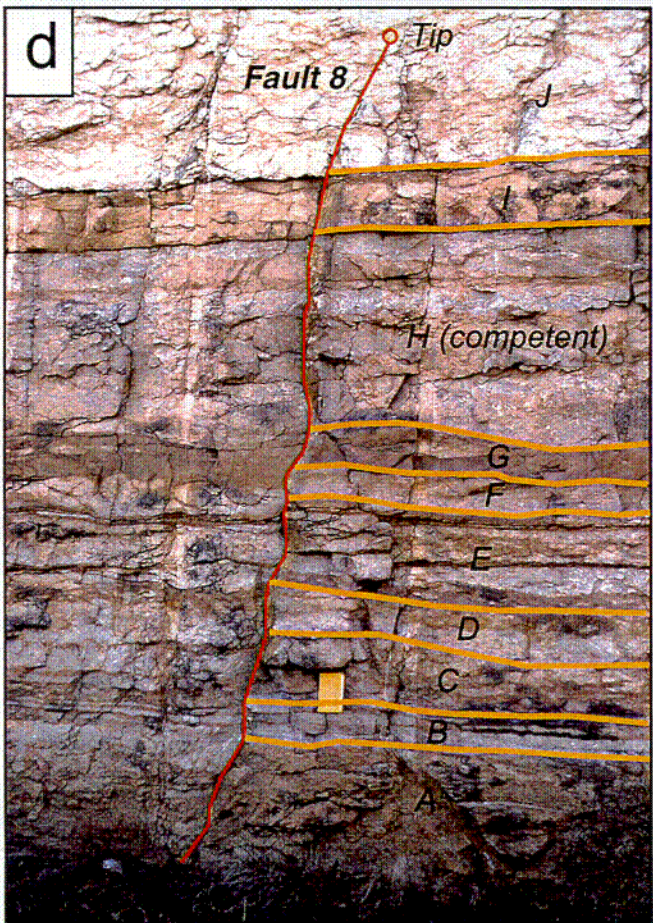
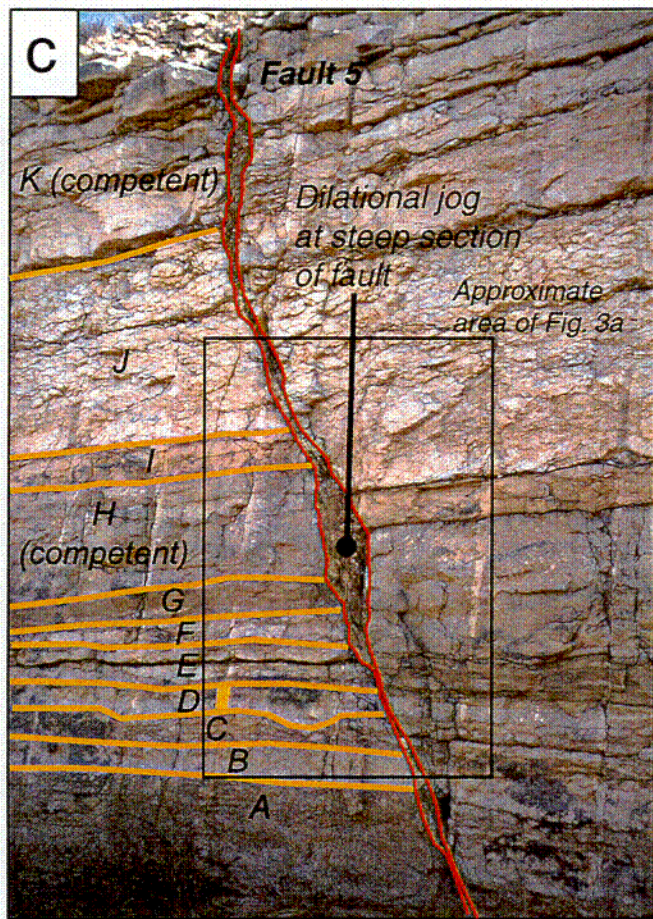
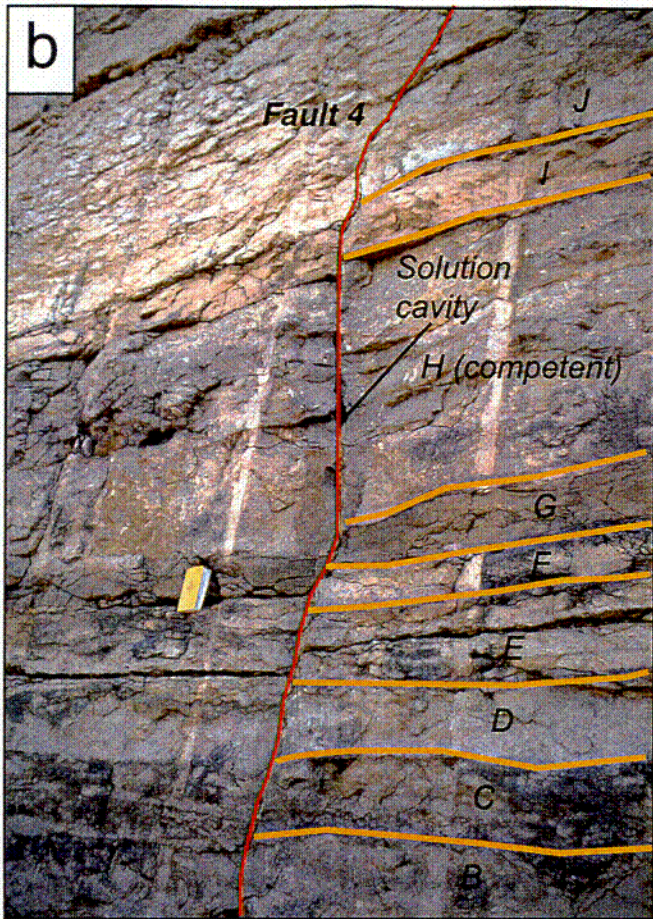
Ferrill & Morris
 Fig. 1



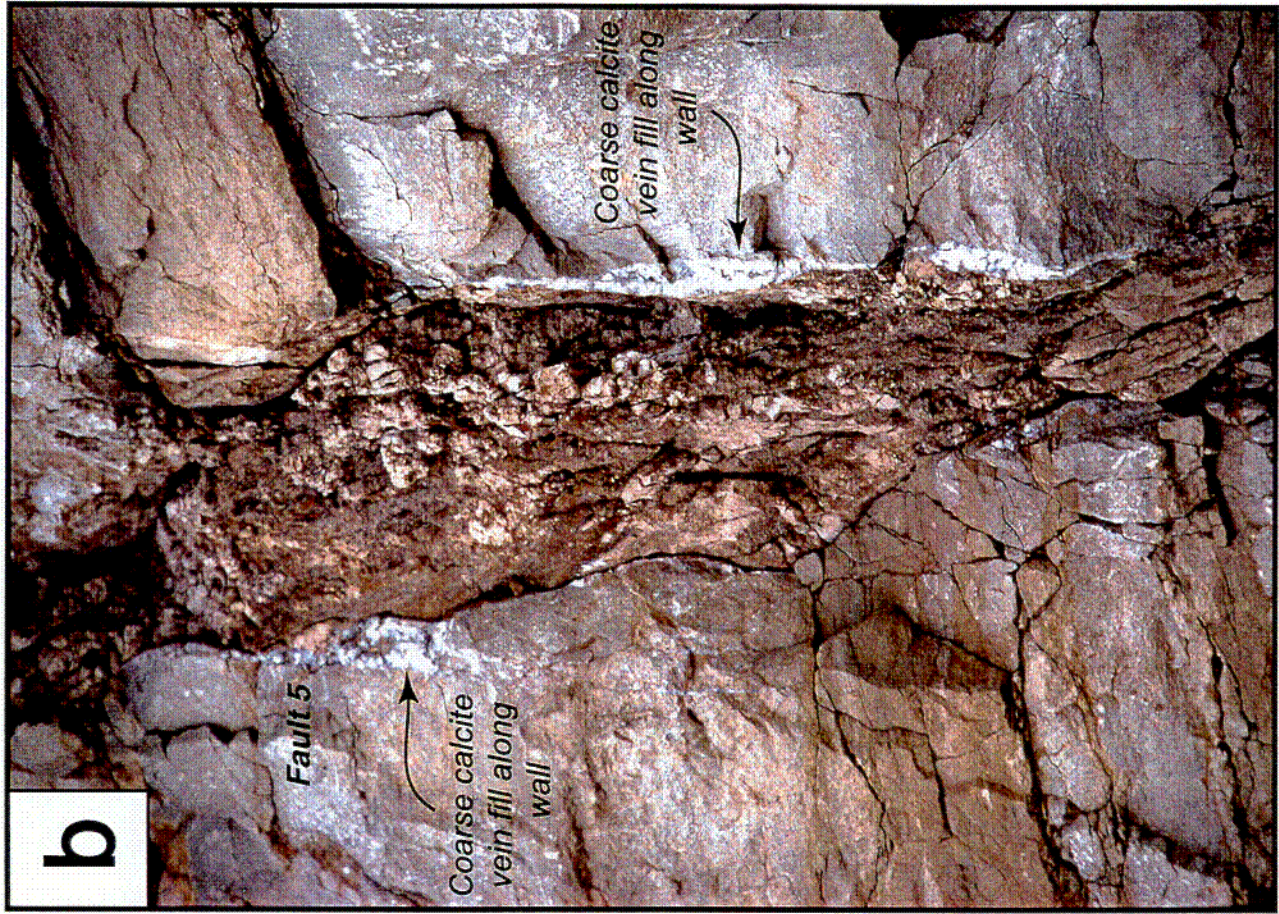
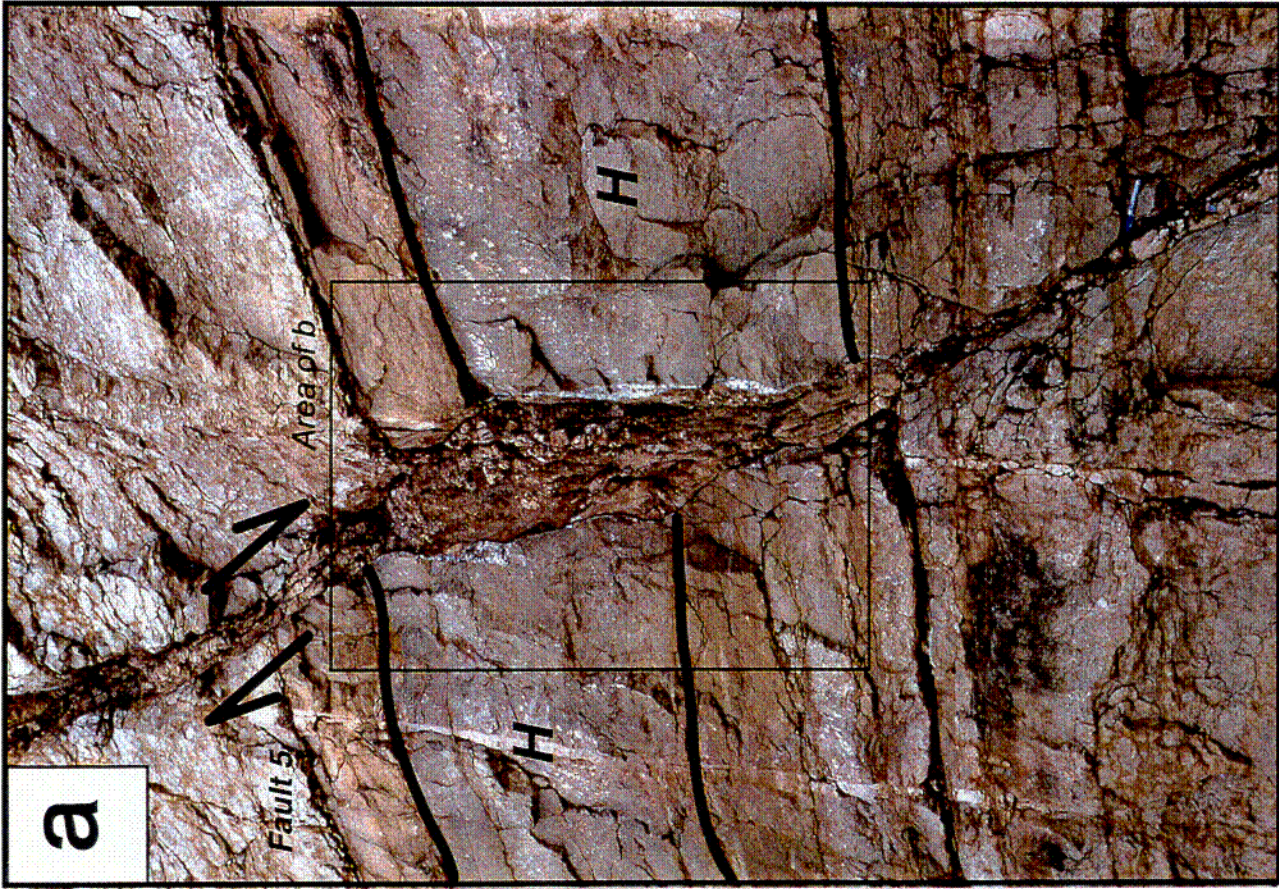
a

CD1

Fig. 2a
Ferrill & Morris

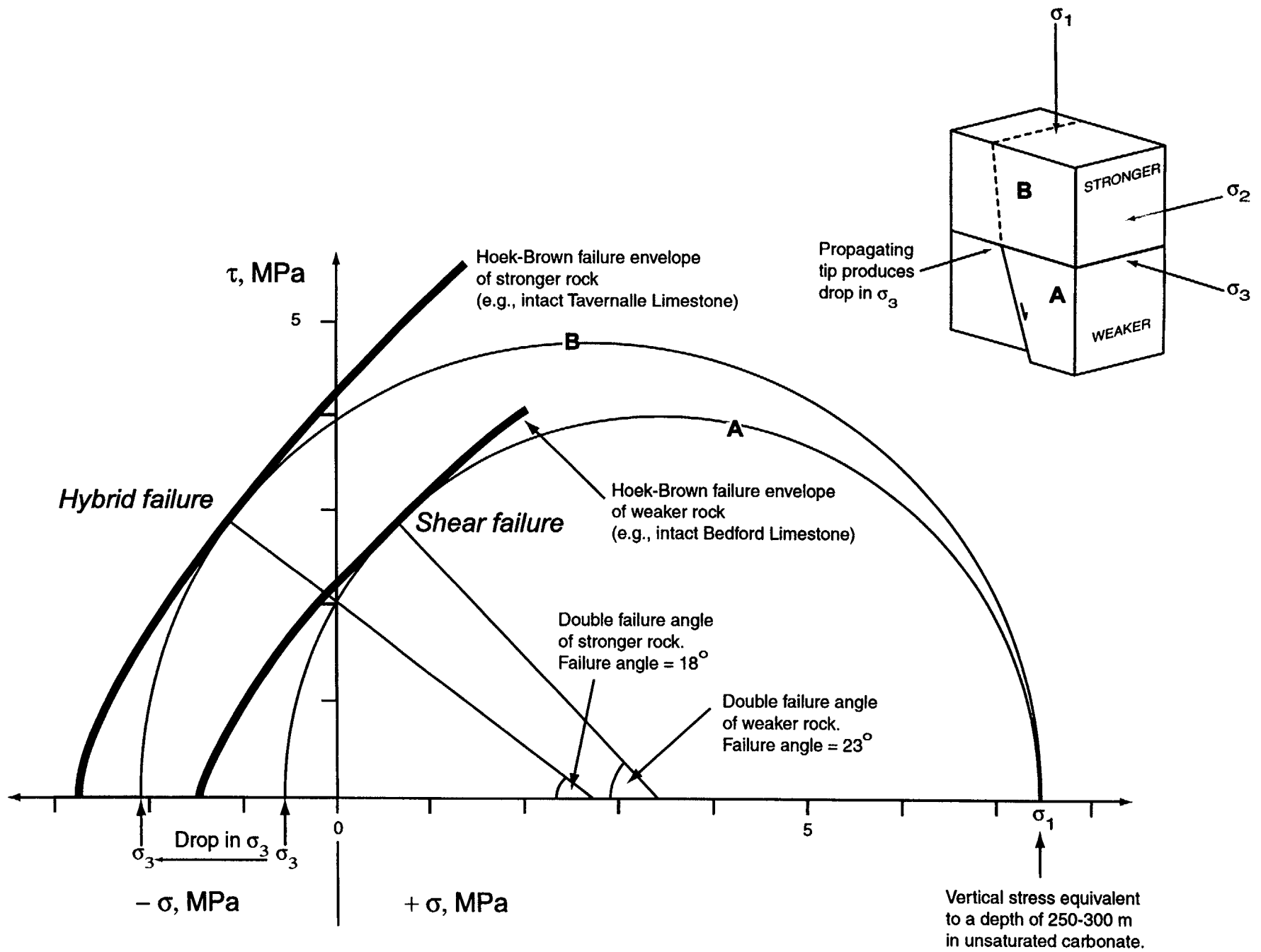


002 Fig. 2b,c,d,e
 Ferrill & Morris

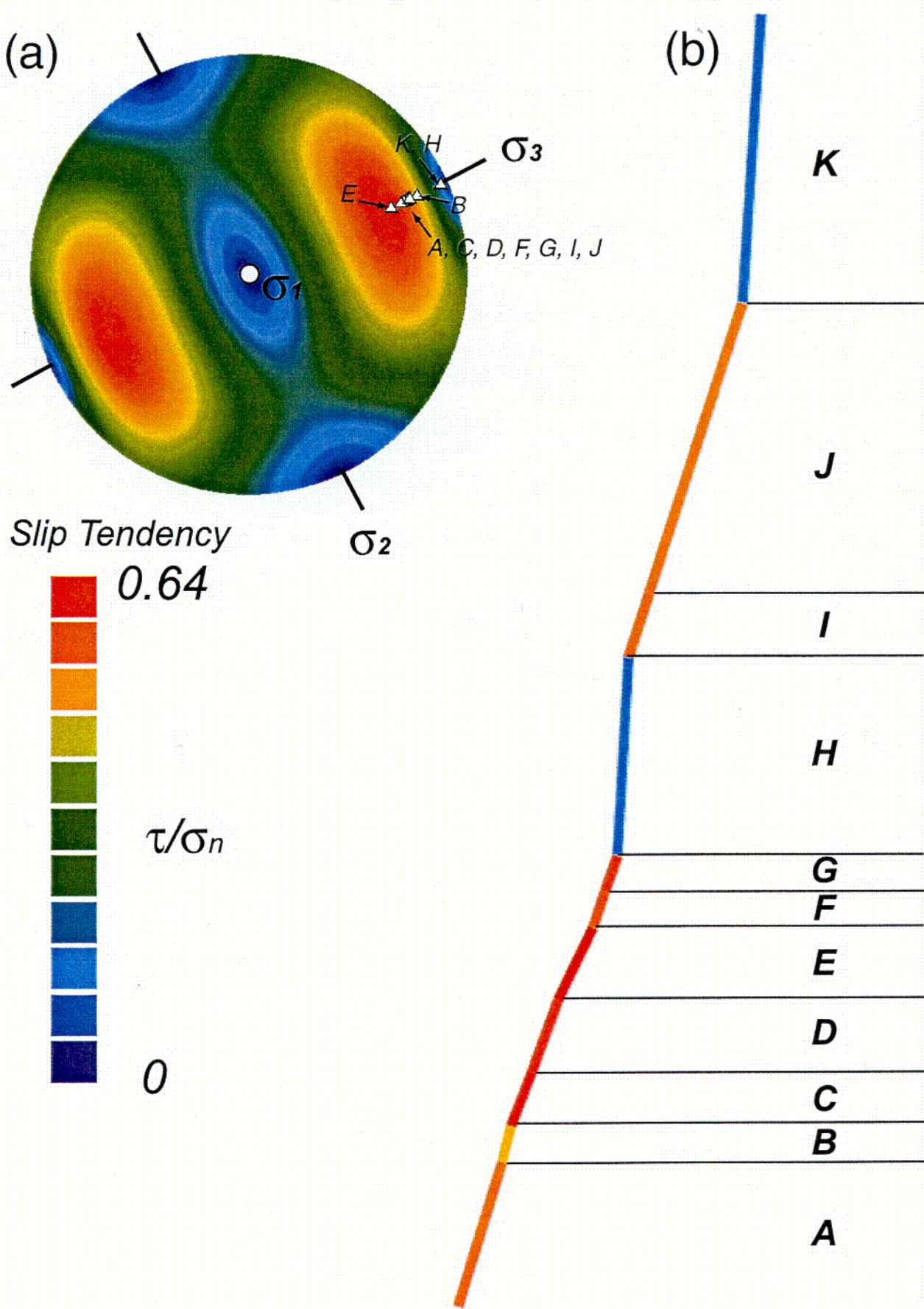


203

Fig. 3
Ferrill & Morris



Ferrill & Morris
Fig. 4



004

Fig. 5
Ferrill & Morris

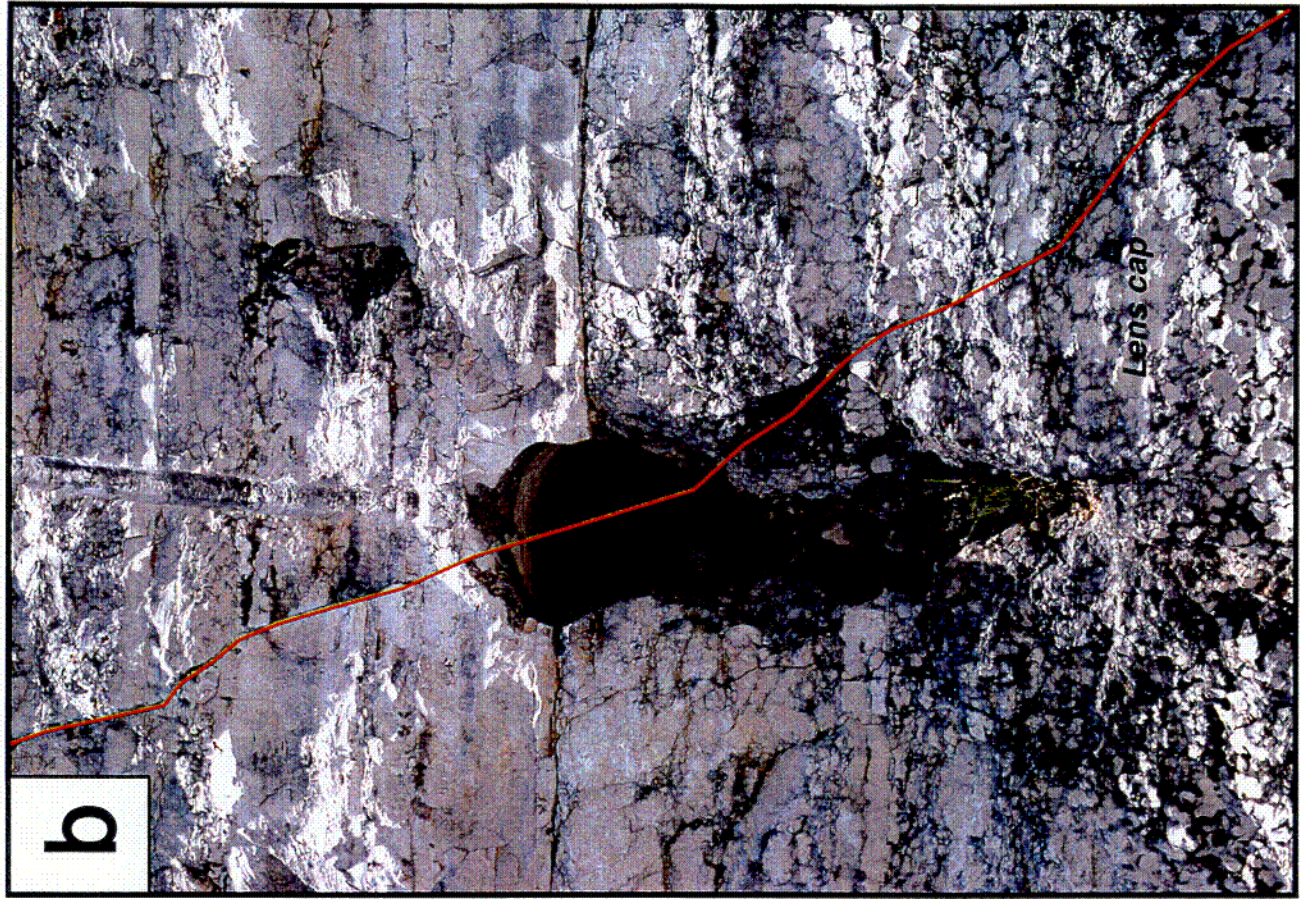
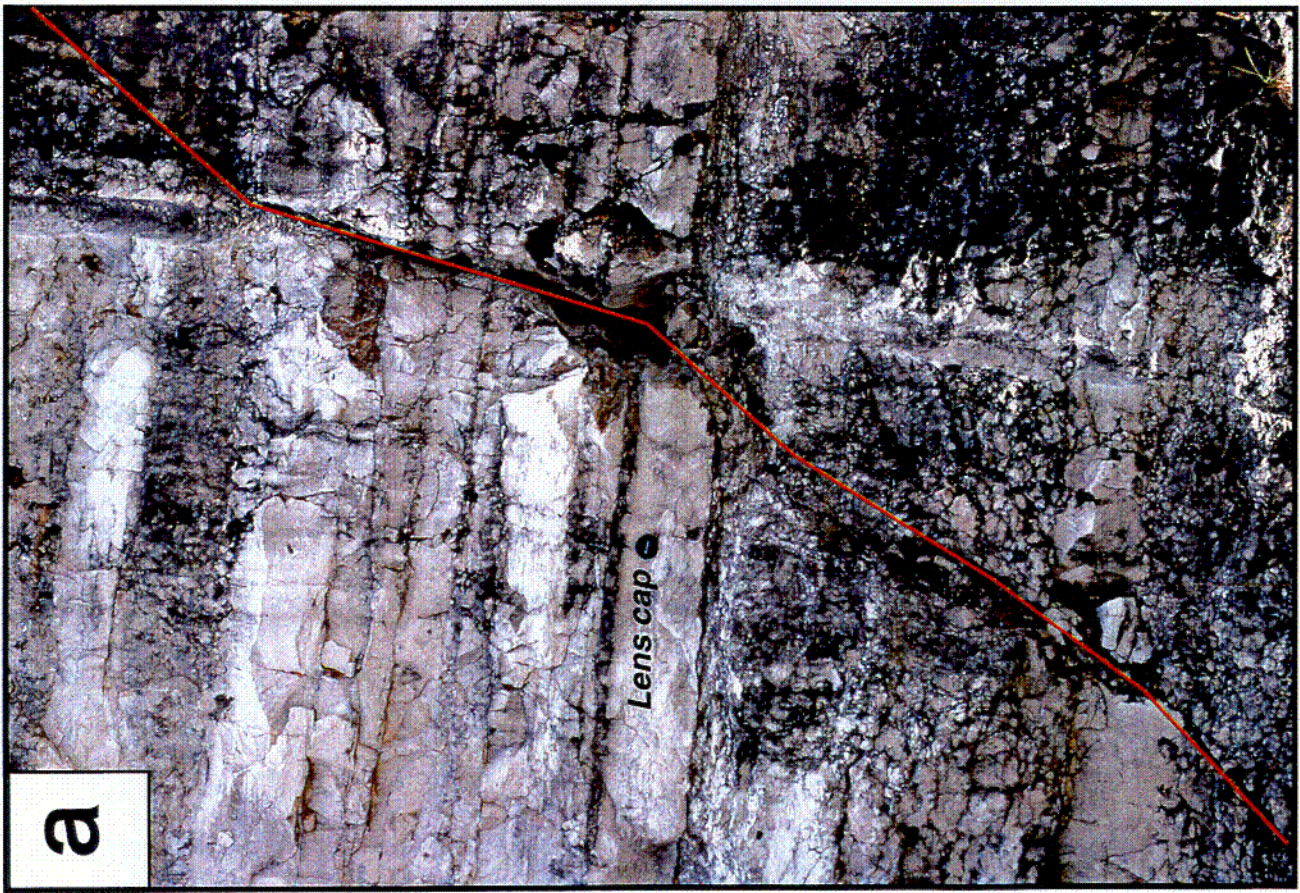


Fig. 6
Ferrill & Morris

C05

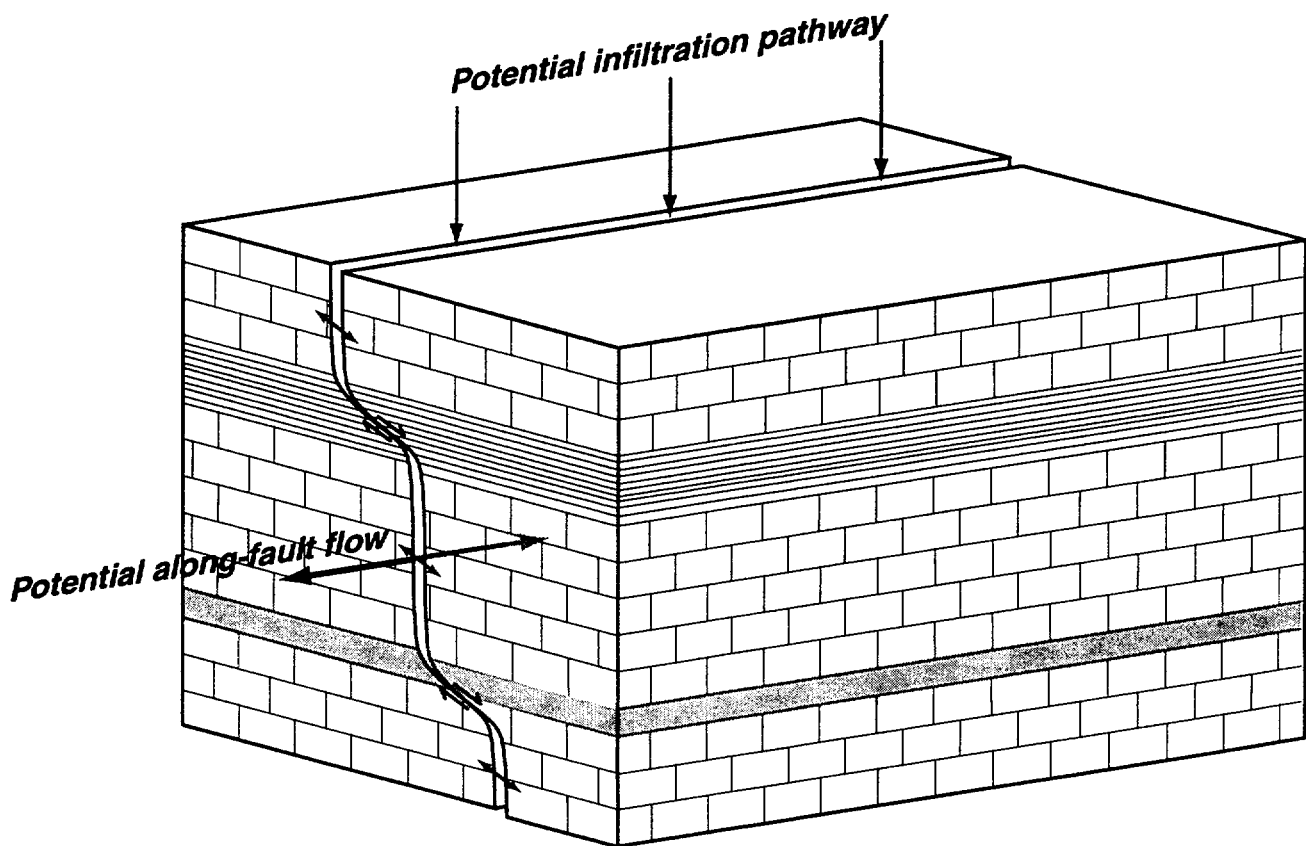


Fig. 7
Ferrill & Morris

Table 1.

Bed	Fault strike	Fault Dip	Bedding Strike	Bedding Dip	Corrected Fault Strike	Corrected Fault Dip	Failure Angle	
Fault 4								
K (competent)	149	82	318	5	149	87	3	
J	329	70	318	5	329	65	25	
I	327	83	318	5	327	78	12	
H (competent)	148	83	318	5	148	88	2	
G	330	71	318	5	330	66	24	
F	329	83	318	5	329	78	12	
E	329	83	318	5	329	78	12	
D	327	79	318	5	327	74	16	
C	327	79	318	5	327	74	16	
B	327	79	318	5	327	74	16	
A	327	79	318	5	327	74	16	
Fault 5								
K (competent)	149	90	318	4	329	86	4	
J	149	72	318	4	149	76	14	
I	149	72	318	4	149	76	14	
H (competent)	149	85	318	4	149	89	1	
G	161	64	318	4	161	68	22	
F	161	64	318	4	161	68	22	
E	161	64	318	4	161	68	22	
D	161	64	318	4	161	68	22	
C	179	70	318	4	179	74	16	
B	179	70	318	4	179	74	16	
A	168	62	318	4	168	66	24	
Fault 8								
K	Above tip		318	5				
J	328	65	318	5	328	60	30	
I	328	79	318	5	328	74	16	
H (competent)	328	86	318	5	328	81	9	
G	328	65	318	5	328	60	30	
F	148	86	318	5	328	89	1	
E	328	65	318	5	328	60	30	
D	148	88	318	5	328	87	3	
C	328	64	318	5	328	59	31	
B	328	81	318	5	328	76	14	
A	328	76	318	5	328	71	19	
Fault 10								
K	Above tip		318	5				
J	145	87	318	5	325	88	2	
I	145	56	318	5	145	61	29	
H (competent)	145	84	318	5	145	89	1	
G	145	84	318	5	145	89	1	
F	155	46	318	5	155	51	39	
E	155	46	318	5	155	51	39	
D	155	46	318	5	155	51	39	
C	152	63	318	5	152	68	22	
B	155	75	318	5	155	80	10	
A	155	75	318	5	155	80	10	
Averages								
	Lithologies						Bed Thickness (cm)	
K (competent)	bedded to moderately massive fossiliferous packstone/wackstone						86.5	3.5
J	fossiliferous wackstone, wavy to sutured stylolites common, shaley base						72.25	17.75
I	calcareous sandstone						72.25	17.75
H (competent)	massive, highly fossiliferous, poorly sorted, spar cemented grainstone						86.75	3.25
G	buff wackstone/packstone						70.75	19.25
F	gray packstone/wackstone						71.5	18.5
E	buff colored wackstone/packstone						64.25	25.75
D	gray packstone/grainstone						70	20
C	buff colored wackstone/packstone						68.75	21.25
B	gray packstone/grainstone						76	14
A	buff colored wackstone/packstone						72.75	17.25